

POLARON: Precision-aware On-device Learning and Adaptive Runtime-cONfigurAble AI acceleration

Mukul Lokhande*, Santosh Kumar Vishvakarma*

*NSDCS Research Group, Indian Institute of Technology Indore, India

Email: skvishvakarma@iiti.ac.in (Corresponding Author)

Abstract—The increasing complexity of AI models requires flexible hardware capable of supporting diverse precision formats, particularly for energy-constrained edge platforms. This work presents PARV-CE, a SIMD-enabled, multi-precision MAC engine that performs efficient multiply-accumulate operations using a unified data-path for 4/8/16-bit fixed-point, floating-point, and posit formats. The architecture incorporates a layer-adaptive precision strategy to align computational accuracy with workload sensitivity, optimizing both performance and energy usage. PARV-CE integrates quantization-aware execution with a reconfigurable SIMD pipeline, enabling high-throughput processing with minimal overhead through hardware-software co-design. The results demonstrate up to 2× improvement in PDP and 3× reduction in resource usage compared to SoTA designs, while retaining accuracy within 1.8% FP32 baseline. The architecture supports both on-device training and inference across a range of workloads, including DNNs, RNNs, RL, and Transformer models. The empirical analysis establish PARV-CE incorporated POLARON as a scalable and energy-efficient solution for precision-adaptive AI acceleration at edge.

Index Terms—Deep learning accelerators, Trans-precision Computing, single instruction multiple data (SIMD) processing elements, Posit precision, Floating-point multiply-accumulate (MAC) operations.

I. INTRODUCTION

THE Artificial Intelligence (AI) landscape has witnessed rapid growth, fueled by the emergence of generative applications such as image manipulation, reinforcement learning (RL), and text-to-image/video generation [1], [2]. Initially designed to automate fundamental tasks such as image classification and data augmentation, particularly deep neural networks (DNNs) has evolved into a powerful tool that augments human creativity and enables intelligent decision making. This progress has accelerated the adoption of AI on mobile and Internet of Things (IoT) platforms, where stringent power, memory, and bandwidth constraints [3], [4] pose significant challenges for real-time inference and on-device learning as visible from Fig. 1. To meet these demands, Modern AI workloads increasingly rely on specialized accelerators offering improved energy efficiency, lower latency, and compact area footprints compared to traditional CPUs. Architectures

This work was supported by the Special Manpower Development Program for Chip to Startup (SMDP-C2S), Ministry of Electronics and Information Technology (MeitY), Govt. Of India. We acknowledge the use of ChatGPT (OpenAI, 2025) for proofreading, grammar correction, and language refinement to improve readability in the early drafts of this manuscript. All technical content, analyses, and results are solely the original contributions of the authors.

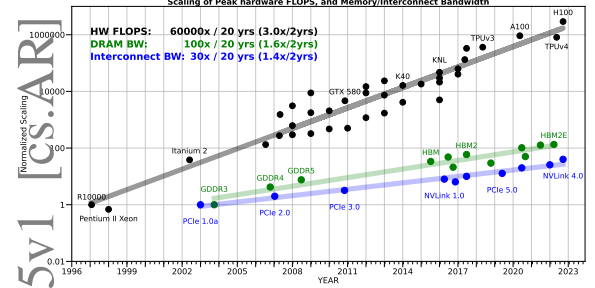


Fig. 1. Decades-long growth in hardware FLOPS, DRAM, and interconnect bandwidth, emphasizing the breakdown of Dennard Scaling and the need for precision-aware compute under the Roofline model. Adapted from [4]

such as TPUs, GPUs, and custom ASICs or FPGAs are co-optimized across hardware and software layers using model compression, architectural innovations, and alternate number systems [5]. Nonetheless, deploying within tight resource budgets of embedded platforms remains non-trivial, bottlenecked by transmission bandwidth.

Multiply-accumulate (MAC) operations dominate the computational workload in DNNs [6], accounting for over 90% of total operations particularly within Convolutional layers or multi-layer perceptron (MLP). For instance, the VGG-16 architecture requires approximately 15.5G MACs, whereas large transformer models such as GPT-3 demand over 6.7T MACs. Thus, the resource-efficient design and optimization of MAC units becomes critical to enhance system-level throughput. However, implementing multiplexed separate-precision data-paths incurs significant hardware overhead and leads to dark silicon [10], [14]. Trans-Precision computing, with dynamic adjustment of precision formats and data widths, has proven effective in enhancing resource efficiency without

TABLE I
STATE-OF-THE-ART (SOTA) COMPUTING APPROACHES AND RESPECTIVE FEATURES IN MULTIPLY-ACCUMULATE COMPUTE ENGINES

Design	Computing	Bit-width	Datatypes	Limitations	Applications
TVLSI'25 [6]	Multi-Precision	4/8/16/32	FxP	Memory-bound	FPGA
TCAD'25 [7]	Mixed-Precision	4/8/16/32	FP/BF/TF	Memory-bound	FPGA
TCAS-II'24 [8]	Mixed-Precision	2/4/8/16/32	INT/FP/BF/TF	Memory-bound	HPC
HCS'24 (NVIDIA)	Mixed-Precision	4/6/8/16	FP/BF	-	GPU
TCAD'24 [9]	-	16/32	FP/HFP/BF/TF	Compute-bound	HPC
TCAS-II'24 [10]	Mixed-Precision	16/32/64	FP/TF/BF	Compute-bound	HPC
Micro'24 (AMD)	Mixed-Precision	4/8/16/32	INT/BF	Memory-bound	PC / Desktop
IoT'24 [11]	Mixed-Precision	2/4/8	FxP	Compute-bound	edge AI
JSSC'23 [12]	Multi-Precision	4/8/16	INT/FP	Compute-bound	Mobile AI
ESSCIRC'23	Mixed-Precision	4/8	FP	Compute-bound	DNN Training
TCAS-II'22 [13]	Multi-Precision	8/16/32	FP/Posit	Memory-bound	-
ISCA'21 (IBM)	Mixed-Precision	2/4/8/16	FP/FxP	-	DNNs
TC'20	Multi-Precision	1/2/4/8/16/32	FP/FxP	Memory-bound	DNN Training
Proposed	Trans-Precision	4/8/16	FP/Posit/FxP	Runtime-adaptable	On-device Learning AI workloads

compromising application accuracy, particularly by enabling selective use of lower-precision computations [15]–[17]. Our work investigates hardware support for the same, to enable efficient on-device learning (ODL) acceleration under resource constraints across diverse AI workloads. Table I presents a comprehensive summary of recent commercial computing devices, with detailed analysis of integrated MAC units such as computing type, bit-width, data format, performance limitations, and target applications. Notably, the proposed work stands out as the first to offer runtime-adaptable trans-precision computation across all fixed-point (Fxp), floating-point (FP), Posit formats and 4/8/16-bit precision. This versatility enables efficient deployment across a wide range of AI workloads, including DNNs, transformers, RL, and generative AI applications.

The primary contributions are summarized as follows:

- **Precision-Aware Runtime-adaptive Vector Compute Element (PARV-CE):** This work introduces enhanced-performance, precision-aware on-device learning CE, which supports adaptive, runtime-configurable throughput up to 16× for Var-Fxp4 and Var-FP8 (E5M2, E4M3), 4× for Var-Fxp8, Posit8, and BF16, and 1× for Var-Fxp16, Posit16, and Var-FP16 (E5M10, E6M9). This is enabled through a resource-shared MAC architecture that maintains near 100% hardware utilization.
- **WILD-QLite Quantization Algorithm:** A novel distribution-aware quantization framework that dynamically adjusts bit-widths based on workload sensitivity and layer criticality to maximize hardware efficiency. Co-designed with a configurable multi-port memory architecture, the algorithm enables parallel data access and optimized resource utilization, supporting low-precision training and inference with minimal accuracy degradation.
- **Resource-Efficient POLARON Edge-AI Engine Analysis:** An empirical performance evaluation of the enhanced POLARON Edge-AI engine is presented, highlighting the impact of runtime-adaptable precision formats and data widths on application performance and hardware resource utilization.

II. CONCEPTUALIZATION : POLARON EDGE AI ENGINE

A. PARV-CE : MAC Compute Unit

Several commercial efforts [15]–[17] have focused on the development of SIMD-MAC units, supporting multi-precision product accumulation, with shared data-paths to enhance resource efficiency and throughput, for AI-ML applications. The prior works [7]–[10], [13] primarily decomposed compute data-path into multiple pipeline stages such as input processing, sign handling, exponent/regime processing, mantissa multiplication, output accumulation, and final output formatting depending on the precision involved, latency to be achieved and hardware efficiency. We designed our compute unit as a five-stage pipelined architecture, with similar processing phases - ranging from input pre-processing to final output

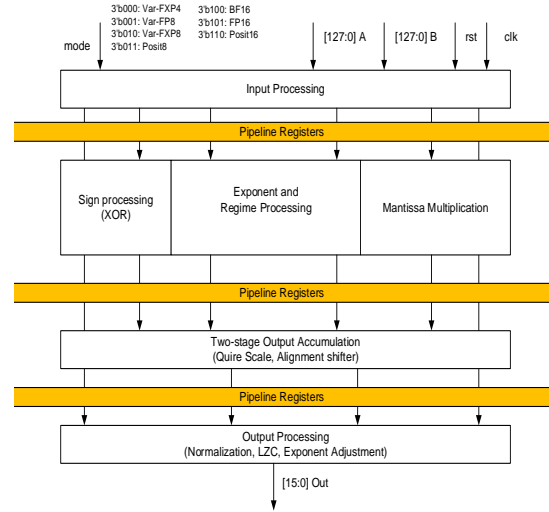


Fig. 2. The detailed micro-architecture of 5-stage Precision-Aware Runtime-adaptive Vector Compute Element (PARV-CE) for enhanced-performance ON-device learning

handling, while focused on low-latency and area-efficiency. What differentiates this work is comprehensive support for diverse precision formats is Var-Fxp4/8 for DNNs, RNNs, and reinforcement learning (RL); FP8 for large language models (LLMs); Posit-8 and Posit-16 for training; and BF16 for general-purpose AI computations enabling efficient and flexible on-chip execution across a wide range of AI workloads.

Variable Precision Processing: The Posit-16 fused MAC data-path is architected to support morphable SIMD-precision, enabling runtime adaptation to various input formats as per the specified operating modes. The design efficiently manages scale factors and minimizes hardware overhead, similar to [13]. The input processing block (Stage-I) performs the unpacking of operands by extracting the sign, exponent/regime, and mantissa fields, and route to respective computational units. To support variable bit-widths across different precision modes, a non-unified memory access scheme is employed using a configurable multi-port memory architecture. The architectural integration through an adaptive, precision-aware data pre-fetcher and configuration subset controller, ensuring efficient data handling and processing across modes.

Runtime adaptive SIMD Multiplication: Stage II performs vectorized multiplication using 16x 4-bit modified radix-2 Booth multipliers and supports reconfigurable operation across multiple precision modes, similar to [8]. Exponent comparison and regime processing are implemented using a simplex multiplexer-based architecture. The datapath dynamically reallocates resources to balance throughput and precision, enabling efficient execution for varying operand widths. Var-Fxp4 uses 4-bit multipliers, Var-FP8 combines 4-bit exponent and mantissa processing, while Posit8, Var-Fxp8, and BF16 utilize 8-bit multipliers. Exponent outputs and mantissa products are realigned via a Quire accumulation. It also contains the simultaneous exponent comparison logic and partial products to fed to signed adder tree.

Two-stage accumulation: Stage III, exponent difference from prior stage are aligned against the maximum exponent.

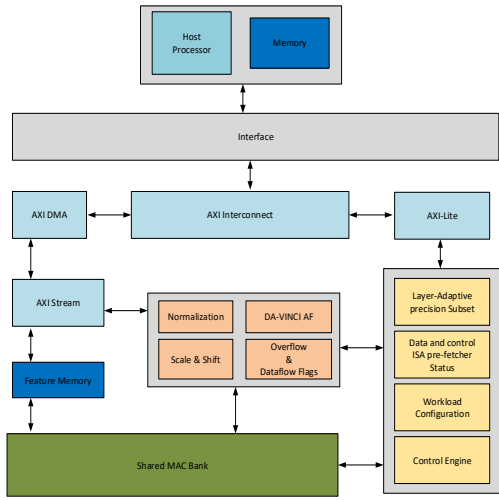


Fig. 3. Proposed Precision-aware On-device Learning and Adaptive Runtime-Configurable (POLARON) edge-AI Engine.

Depending on sign bits, 2's complement is applied to the partial products. These aligned values are passed through a shifter and into a two-stage adder tree: Stage I (S3) implements a 4:2 Carry-Save Adder (CSA), while Stage II (S4) finalizes the summation using an additional CSA and a Carry-Select Adder (CSLA). Depending on the accumulation configuration, this stage ensures correct handling of partial sums and supports an optional Kulisch-style accumulation [7]. This technique enables zero-passing based on the sign bit and selectively skips accumulation operations, thereby accelerating training.

Output Inter-format Restructuring: This stage performs normalization and rounding on the accumulated output. A Leading Zero Anticipator (LZA) determines the required shift for normalization, followed by adjustment of the exponent and mantissa. Rounding is carried out using the RoundTowardPositive method [18], which simplifies hardware implementation and mitigates underestimation errors caused by exponent-induced truncation. The final output is composed of sign, exponent, and mantissa fields in floating-point mode, or a regularized mantissa in fixed-point mode.

B. WILD-Q Lite Quantization Algorithm

Prior works [5], [6], [19]–[21] have demonstrated on-device implementations of various AI workloads using precision-aware formats like DNN inference/training with Var-FxP4/8; Encoder/Decoder with Var-FxP8; RNNs, LSTMs, and Transformers with FP8; reinforcement learning with FxP8/16. Additionally, Posit-8 (\sim FP16), Posit-16 (\sim FP32), and BF16 have been shown to offer sufficient precision [22] for a wide range of AI workloads on hardware. The Hybrid Layer-Adaptive Precision Framework [6] enables efficient AI execution across heterogeneous edge platforms by decoupling neural architecture search (NAS) from the training phase and supporting the deployment of specialized sub-networks through structured pruning of depth, width, kernel size, and input resolution - Without requiring retraining from scratch. Building on this principle, we propose a unified, precision-aware execution

framework that supports a broad range of AI workloads, governed by a layer-adaptive precision subset. The proposed architecture employs a mixed-precision strategy integrated within the **PARV-CE** (Precision-Aware Runtime-Vectorized Compute Engine), which achieves competitive accuracy with less than 1.8% degradation while significantly enhancing resource efficiency. Specifically, the framework utilizes Var-FxP4/8 for DNN inference and training, Var-FxP8 for encoder-decoder models, FP8 for RNNs, LSTMs, and Transformers, and FxP8/16 for reinforcement learning. In addition, it supports Posit-8 (comparable to FP16), Posit-16 (comparable to FP32), and BF16 for general-purpose AI tasks.

The quantization-aware training (QAT), incorporating layer-wise precision sensitivity analysis is adapted to preserve application accuracy. For the l^{th} layer, the sensitivity metric s_l to quantify the impact of precision on gradient magnitude:

$$s_{l_{sc},k} = \frac{\left(\|Q^{\text{Ad-P}}(\mathbf{w}_l) - \mathbf{w}_l\| - \|Q_{sc,k}^{\text{Ad-P}'}(\mathbf{w}_l) - \mathbf{w}_l\| \right) \times \|\nabla \mathcal{L}_{\mathbf{w}_l}\|}{n_l} \quad (1)$$

with

$$s_l = \max(s_{l_{sc,8}}, s_{l_{sc,4}}). \quad (2)$$

where $Q^{\text{Ad-P}}(\cdot)$ denotes the adaptive precision quantization function, $\nabla \mathcal{L}_{\mathbf{w}_l}$ is the loss gradient with respect to weights \mathbf{w}_l , and n_l is the number of weights in layer l . Unlike traditional symmetric ranges (e.g., $[-1, 1]$), the scheme dynamically adjusts the saturation thresholds W_l and W_h based on the learned weight distribution. The quantization process involves computing a scale factor:

$$\text{scale}(k) = \text{mean}(|W|) \cdot \frac{2^n - 1}{2^{n-1}}, \quad (3)$$

$$\widehat{W} = \text{round} \left(\left(\text{clip} \left(\frac{W}{k}, W_l, W_h \right) - W_l \right) \cdot \frac{2^n - 1}{W_h - W_l} \right), \quad (4)$$

$$Q^{\text{Ad-P}}(W) = \widehat{W} \cdot \frac{W_h - W_l}{2^n - 1} + W_l, \quad (5)$$

where n denotes the quantization bit-width and W is the original weight value. The resulting quantized representation is aligned with the model's statistical characteristics, enabling efficient deployment across variable-precision hardware, similar to [6], [23]. The framework leverages the parameterized clipping activation (PACT) function, which enables learnable thresholding during training:

$$y = \text{PACT}(x) = 0.5(|x| - |x - \alpha| + \alpha). \quad (6)$$

$$x^q = \text{round} \left(y \times \frac{2^n - 1}{\alpha} \right) \times \frac{\alpha}{2^n - 1}. \quad (7)$$

where α is the learnable clipping parameter. This approach mitigates quantization-induced accuracy loss by maintaining a balanced distribution around zero, while QAT compensates for approximation errors, preserving higher precision only in critical layers. Overall, the proposed framework enables efficient AI deployment on edge devices by combining quantization-aware training, entropy-based bit-width allocation, and layer-wise precision tuning to achieve high accuracy with improved resource efficiency.

C. POLARON Architecture

The proposed POLARON architecture presents a precision-adaptive accelerator designed to support efficient execution of AI workloads on edge platforms. At the heart of the design is a shared MAC bank, which performs varying precision MAC compute in Var-FxP4/8/16, Var-FP8, BF16, and Posit-8/16. Data ingress and egress are managed through an AXI interconnect, which bridges communication between the host processor/memory subsystem and the accelerator via AXI-Lite for configuration and AXI-DMA/Stream for high-throughput feature transfers. Incoming data is temporarily stored in the Feature Memory, to stage before feeding to MAC units. The architecture supports runtime adaptability via a layer-adaptive precision subset, enabling per-layer precision tuning for optimal trade-offs between accuracy and efficiency.

Post-processing with separate block includes normalization, scale-and-shift, overflow detection, and a custom CORDIC-driven DA-VINCI AF unit, which supports Swish, SoftMax, SeLU, GELU, Sigmoid, Tanh, ReLU. These modules ensure dynamic range alignment, prevent numerical saturation, and enable nonlinear transformations required for deep neural network layers. Control and coordination are managed by a runtime control engine that interfaces with a workload configuration module and a data/control ISA pre-fetcher, allowing preemptive adjustment of execution parameters based on layer-specific metadata. This tightly coupled data-flow-centric design ensures minimal latency, efficient memory utilization, and precision-aware computation tailored to the demands of modern AI workloads.

III. PERFORMANCE ANALYSIS

The performance evaluation of the proposed DNN accelerator follows a comprehensive co-design methodology, integrating software-based accuracy analysis with hardware-aware architectural modeling. An iso-functional emulation of the custom MAC arithmetic was implemented in Python 3.0 using the FxP-Math package and QKeras 2.3, executed within a Jupyter Notebook environment on an NVIDIA V100 GPU. The evaluation spans multiple precision and format with FP32 baseline. A diverse set of models was assessed under edge inference scenarios. The results demonstrate that the proposed WILD-QLite quantization framework sustains high model fidelity, with less than 1.8% degradation in accuracy and a Quality of Results (QoR) score exceeding 98.5%, validating its suitability for precision-constrained edge deployment.

The proposed PARV-CE and POLARON architecture were modeled in Verilog HDL with programmable support for multiple precision modes, demonstrating the flexibility. Functional verification was conducted using the QuestaSim simulator, with outputs cross-validated against the Python-based software emulation framework. FPGA synthesis and implementation were performed using the AMD Vivado Design Suite, and detailed resource utilization results are provided in Table II and Table V. Additionally, all designs were synthesized using Synopsys Design Compiler targeting the TSMC 28nm technology node, with corresponding post-synthesis performance metrics

TABLE II
FPGA RESOURCE UTILIZATION FOR SoTA MAC DESIGNS

Design	Precision	FPGA Utilization (Virtex 707)				
		LUTs	FFs	Delay (us)	Power (mW)	Arith. Intensity (p/Op)
AMD IP (FPGA)	FxP4	53	28	3.09	3.48	10.75
	FxP8	130	44	3.816	7.26	27.7
	FxP16	369	76	9.051	16.9	153
	FxP32	1426	214	5.931	22	130.4
TVLSI'25 [6]	FxP8	256	224	5.98	9.23	55.2
	FxP16	427	369	6.5	11.78	76.57
	FxP32	681	745	7.34	31	227.54
	SIMD-Pipelined	897	1231	11.7	59.4	694
ISCAS'25 [22]	Posit8	467	175	2.68	68	182.24
	Posit16	2083	528	4.35	189	822.15
	Posit32	6813	806	8	347	2776
	SIMD-L-Posit	4613	2078	6.2	276	426
TCAS-II'24 [8]	SIMD-INT4/FP8/16/32	8054	1718	4.62	296	152
TVLSI'23 [18]	SIMD-FP16/32/64	8065	1072	5.56	378	543
Access'24 [25]	Q-4b	24	16	0.98	2.2	2.16
	Q-8b	52	88	1.57	6.36	10
	Q-16b	106	168	2.2	11.77	26
	Vector Q-MAC (FxP-8/16/32)	1502	2418	40.32	21.38	108
TCAS-I'22 [26]	FxP8	238	32	2.75	2.8	7.6
TRETS'23 CORDIC [24]	FxP4	35	58	1.406	4.36	6.13
	FxP8	54	88	1.518	6.6	10
	FxP16	95	162	2.124	12.21	25.9
Baseline	Ad-FxP-4/8/16,	875	1134	10.89	54.7	37.23
Proposed	Var-FP8/16, Posit8/16	326	182	2.89	31.67	5.72

TABLE III
ASIC PERFORMANCE COMPARISON OF SoTA MAC DESIGNS

Design	Tech. nm	Voltage V	Freq GHz	Area mm ²	Power mW
TVLSI'25 [6]	28	0.9	1.36	0.049	7.3
ISCAS'25 [22]	28	0.9	1.12	0.024	32.68
TCAS-II'24 [8]	28	1	1.47	0.010	15.87
TCAD'24 [9]	28	1	1.47	0.024	82.4
TCAS-II'24 [10]	28	1	1.56	0.022	72.3
TCAS-II'22 [13]	28	1.05	0.67	0.052	99
TVLSI'23 [14]	28	1	2.22	0.013	59.3
TVLSI'22 [18]	28	1	1.43	0.013	29.3
Baseline	28	0.9	1	0.062	112
Proposed	28	0.9	1.86	0.011	28.2

reported in Table III, Table IV and Table VI. To ensure a fair comparison, several prior SoTA designs were re-implemented under identical experimental conditions. Results from both FPGA and ASIC implementations confirm that the proposed architecture achieves significant improvements in performance and resource efficiency over existing approaches.

The proposed PARV-CE shows significant improvements in efficiency and scalability across both FPGA and ASIC platforms. On FPGA (Table II), demonstrates lower resource utilization and power consumption while delivering competitive throughput, outperforming SoTA designs with almost 2× in PDP and 1.5× in arithmetic intensity. Compared to SIMD-based and high-precision MAC implementations, the proposed design offers broader precision support and maintains consistently high efficiency with minimal logic overhead. On ASIC (Table III), PARV-CE achieved over 1.3× quicker operating frequency and consume 2× smaller area compared to SoTA works, with total consumption reduced by 40–50% relative to prior precision-flexible MACs. Stage-wise analysis (Table IV) further emphasizes these advantages, predominantly arising from a reduction in both area and power across major pipeline stages. This effectively highlights the proposed PARV-CE for

TABLE IV
COMPARISON FOR STAGE-WISE RESOURCES CONSUMED BY DIFFERENT MAC UNITS

	TVLSI'22 [18]		TCAS-II'22 [13]		TVLSI'23 [14]		TCAS-II'24 [10]		TCAD'24 [9]		Proposed	
Stage	Area (μm^2)	Power(mW)	Area (μm^2)	Power(mW)	Area (μm^2)	Power(mW)	Area (μm^2)	Power(mW)	Area (μm^2)	Power(mW)	Area (μm^2)	Power(mW)
Input Pre-proc.	1902	14.5	8079	16.2	6575	24.5	13432	41	14735	45	673	1.78
Mantissa Mult.& Exponent Proc.	5907	45	22772	43.5							3978	9.67
Accumulation	2810	22	13273	26	1540	8.7	5636	20	3058	12	3426	9.2
Output Proc.	2778	21.2	5855	11	4914	26	2849	11.4	6320	25.5	3068	7.52
Total	13397	102.7	49979	96.7	13029	59.2	21917	72.4	24113	82.5	11147	28.2
Op. Freq. (GHz)	1.42		0.67		2.22		1.56		1.47		1.86	

TABLE V
FPGA RESOURCES COMPARISON WITH SoTA ACCELERATOR ARCHITECTURES [6], [24], [27]–[30]

	TCAS-I'22 [27]	TCAS-I'22 [28]	TCAD'23 [31]	TRETS'23 [24]	TCAS-II'23 [32]	TVLSI'23 [29]	TCAS-I'24 [30]	TCAS-I'24 [33]	TVLSI'25 [6]	Proposed
Platform	Intel Aria-10	KCU15	ZCU-102	VC707	XCVU9P	ZCU102	ZU3EG	A7-100T	VC707	VC707
Model	MobileNet-v2	YoloV3-tiny	MobileNet-v2	LeNet-5	YoloV3-tiny	XoR-Net	ResNet-50	YoloV3-tiny	VGG-16	YoloV3-tiny
Precision	8	8	8	8/16	8	8	8	8	8/16/32	4/8/16
LUTs	102.6 K	213.3 K	164.4 K	144 K	132 K	117 K	40.78 K	50.2 K	38.7 K	37.2 K
FFs	-	352 K	-	155.8 K	39.5 K	74 K	45.25 K	58.1 K	7.4 K	8.6 K
DSPs	512	2240	1283	23	96	132	257	240	73	-
Freq (MHz)	170	200	333	466	150	300	150	100	466	250
Power (W)	4.6	0.51	0.96	1.54	5.52	6.58	1.4	2.2	2.24	0.93

compact, scalable and faster edge execution.

The effective throughput benefits from PARV-CE and adaptive precision frameworks translate very significantly to POLARON accelerator implementation. As shown in Table V, the FPGA-based design consumes $3\times$ lesser LUTs and FFs compared to SoTA designs, at similar frequency. The use of a trans-precision compute engine enables broad support for mixed-precision formats, including FxP4/8/16 and Posit8/16, which helps reduce logic complexity and improves runtime adaptability. In terms of system-level evaluation (Table VI), POLARON shows 2-4 \times better energy efficiency compared to SoTA designs and better accuracy. The ODT for VGG-16 was observed 4.2% times faster compared to prior works [6]. Overall, the proposed architecture offers a compelling blend of flexibility, accuracy, and efficiency making it an ideal candidate for low-power edge-AI deployments.

The proposed POLARON was deployed for object detection and classification tasks on the Pynq-Z2 platform, utilizing the ARM Cortex-A9 processor as the host CPU. Real-time deployment demonstrates that the proposed system outperforms prior works in both latency and power consumption, achieving 11 fps and 0.8W W on Pynq-Z2, compared to 186.4 ms / 2.24 W for [6] on VC707, 772 ms / 1.524 W for [24] on VC707, 184 ms / 0.93 W for [22] on Pynq-Z2, and baseline values of 226 ms / 1.34 W for Jetson Nano and 555 ms / 2.7 W for Raspberry Pi. The architecture also benefits from early-exit strategy that conditionally skips layers. The inference accuracy for RNNs, LSTMs stays within 1.2% compared to FP32 and RL between 1%. We mark this as an opportunity for future exploration.

IV. CONCLUSION

This work presents POLARON, a precision-aware and runtime-adaptive edge AI accelerator, incorporating the PARV-CE to address the emerging needs of energy-efficient, scalable, and trans-precision AI computation at the edge. It supports unified MAC operations across Var-FxP4/8/16, Var-FP8/16, BF16, and Posit8/16, for diverse AI workloads. With the integration of the WILD-QLite quantization algorithm and

layer-adaptive execution framework, the design achieves improved throughput and resource efficiency, while maintaining model accuracy within 1.8%, compared to FP32 baseline. The comprehensive evaluation across FPGA and ASIC platforms demonstrates up to $2\times$ improvement in PDP, $3\times$ reduction in resource usage, and $4\times$ better energy efficiency compared to SoTA designs. The real-time deployment on the Pynq-Z2 platform confirms the suitability of POLARON for low-power edge inference and training. The empirical assessment place POLARON in next-generation AI systems, to exploit precision scalability, hardware adaptability, and performance efficiency under strict edge constraints.

REFERENCES

- [1] Y. S. Shao, "Next-generation domain-specific accelerators: From hardware to system," in *IEEE CICC*, pp. 1–5, 2024.
- [2] M. Verhelst, L. Benini, and N. Verma, "How to keep pushing ml accelerator performance? know your rooflines!," *IEEE Journal of Solid-State Circuits*, pp. 1–18, 2025.
- [3] J. R. Hu, L. Liu, *et al.*, "Co-Optimization of GPU AI Chip: Technology, Design, System and Algorithms," in *IEEE IEDM*, pp. 1–4, 2024.
- [4] A. Gholami, Z. Yao, *et al.*, "AI and Memory Wall," *IEEE Micro*, vol. 44, no. 3, pp. 33–39, 2024.
- [5] D. Han and A. P. Chandrakasan, "MEGA.mini: A Universal Generative AI Processor with a New Big/Little Core Architecture for NPU," in *IEEE ISSCC*, vol. 68, pp. 1–3, 2025.
- [6] M. Lokhande, G. Raut, and S. K. Vishvakarma, "Flex-PE: Flexible and SIMD Multiprecision Processing Element for AI Workloads," *IEEE Trans. VLSI Syst.*, pp. 1–14, 2025.
- [7] H. J. Damsgaard, K. J. Hoffeld, *et al.*, "Parallel Accurate Minifloat MACCs for Neural Network Inference on Versal FPGAs," *IEEE Trans. Comput.-Aided Design Integr. Circuits Syst.*, pp. 1–1, 2025.
- [8] B. Li, K. Li, *et al.*, "A Reconfigurable Processing Element for Multiple-Precision Floating/Fixed-Point HPC," *IEEE Trans. Circuits Syst. II*, vol. 71, no. 3, pp. 1401–1405, 2024.
- [9] H. Tan, L. Huang, *et al.*, "A Low-Cost Floating-Point Dot-Product-Dual-Accumulate Architecture for HPC-Enabled AI," *IEEE Trans. Comput.-Aided Design Integr. Circuits Syst.*, vol. 43, no. 2, pp. 681–693, 2024.
- [10] H. Tan, J. Zhang, *et al.*, "A Low-Cost Floating-Point FMA Unit Supporting Package Operations for HPC-AI Applications," *IEEE Trans. Circuits Syst. II*, vol. 71, no. 7, pp. 3488–3492, 2024.
- [11] A. Krishna, S. Rohit Nudurupati, *et al.*, "RAMAN: A Reconfigurable and Sparse tinyML Accelerator for Inference on Edge," *IEEE Internet of Things Journal*, vol. 11, no. 14, pp. 24831–24845, 2024.

TABLE VI
EVALUATION METRICS COMPARISON BETWEEN DIVERSE SoTA AI ACCELERATOR DESIGNS

Design	Network Topology	Data-type	Tech	Freq (MHz)	Area (mm ²)	Power (W)	Energy Efficiency (TOPS/W)	Accuracy
JSSC'25 [34]	Vector Systolic Array	Fxp4/8	28nm	172	1.04	0.6	8.33	71.68
	G-VSA			199	2	0.3	3.26	67.2
TVLSI'25 [6]	VGG-16	Fxp4/8/16/32	VC707 (28nm)	466	-	2.24	8.42	84.6
	Systolic Array (8x8)		TSMC-28nm	1435	1.8	0.53	10.83	-
TVLSI'25 [21]	784-200-100-10	Fxp8	ASIC-45nm	588	6.13	0.6	1.48	97.4
	784-256-10				5.86	0.642	1.39	96.73
ISCAS'25 [22]	LeNet-5 (64 PQRE)	Posit-8/16/32	VCU129 (16nm)	46.35	-	0.93	4.54	98.7
			ASU-7nm	1835	0.63	1.2	6.2	-
			TSMC-28nm	1350	2.32	2.8	1.98	-
Access'24 [25]	LeNet-5 (64 Quant-MAC)	Fxp8	Virtex-7	262	-	0.18	3.78	97.2
			CMOS 28nm	1382	1.4	1.86	0.78	-
TCAD'23	Tiny-Yolo v3	Fxp8	XC7VU9P	150	-	5.52	-	72.98
ISSCC'23 [35]	ResNet-20	FP16/32, BF16	22nm FDX	420	1.9	0.123	1.66	92.2
ISCAS'24 [36]	ResNet-50	Fxp4/FP-16/32	28nm	160	1.84	67.4	2.19	77.56
TVLSI'23	XNOR-Net	8b	ZCU102	300	-	6.58	1.52	62.98
TCAS-I'22 [37] (PL-NPU)	ResNet-18	Posit8	28nm	1040	5.28	343	1.625	70.1
TRETS'23 [24]	196-64-32-32-10	Fxp8	VC707 (28nm)	466	-	1.524	4.5	95.06
			CMOS-28nm	826	2.34	0.89	9.28	-
TCAS-I'22 [26]	196-64-32-32-10	Fxp8	VC707 (28nm)	357	-	1.78	8.02	96.59
			CMOS-28nm	1376	1.04	0.62	12.22	-
Baseline	LeNet-5 (64 PARV-CE)	Ad-Fxp-4/8/16,	VC707 (28nm)	196	-	1.38	2.27	98.6
			TSMC-28nm	968	1.23	1.68	8.2	-
	VGG-16 (256 PARV-CE)	Var-FP8/16, Posit8/16	VC707 (28nm)	204	-	1.46	2.23	68.7
Proposed	LeNet-5 (64 PARV-CE)	Ad-Fxp-4/8/16,	TSMC-28nm	1167	3.85	1.8	12.8	-
			VC707 (28nm)	250	-	0.93	7.57	98.3
	VGG-16 (256 PARV-CE)	Var-FP8/16, Posit8/16	TSMC-28nm	1023	0.64	0.88	15.2	-
			VC707 (28nm)	237	-	1.16	5.86	68.7
			TSMC-28nm	1238	2.2	1.2	16.5	-

- [12] J.-S. Park, C. Park, *et al.*, "A Multi-Mode 8k-MAC HW-Utilization-Aware Neural Processing Unit With a Unified Multi-Precision Datapath in 4-nm Flagship Mobile SoC," *IEEE Journal of Solid-State Circuits*, vol. 58, no. 1, pp. 189–202, 2023.
- [13] L. Crespo, P. Tomás, N. Roma, and N. Neves, "Unified Posit/IEEE-754 Vector MAC Unit for Transprecision Computing," *IEEE Trans. Circuits Syst. II*, vol. 69, no. 5, pp. 2478–2482, 2022.
- [14] H. Tan, G. Tong, L. Huang, *et al.*, "Multiple-Mode-Supporting Floating-Point FMA Unit for Deep Learning Processors," *IEEE Trans. VLSI Syst.*, vol. 31, no. 2, pp. 253–266, 2023.
- [15] D. Deng, A. Jebson, *et al.*, "Multiply-accumulate unit for single-instruction/multiple-data instructions," Sept. 2006. US Patent 7,107/305.
- [16] M. Siu and S. Oberman, "Multipurpose functional unit with combined integer and floating-point multiply-add pipeline," Nov. 2011. US Patent 8,051/123.
- [17] M. A. Kennedy and N. Burgess, "Apparatus and method for performing multiply-and-accumulate-products operations," Sept. 2019. US Patent 10,409/604.
- [18] W. Mao, K. Li, *et al.*, "A Configurable Floating-Point Multiple-Precision Processing Element for HPC and AI Converged Computing," *IEEE Trans. VLSI Syst.*, vol. 30, no. 2, pp. 213–226, 2022.
- [19] S. Kim, J. Lee, *et al.*, "TSUNAMI: Triple Sparsity-Aware Ultra Energy-Efficient NN Training Accelerator With Multi-Modal Iterative Pruning," *IEEE Trans. Circuits Syst. I*, vol. 69, no. 4, pp. 1494–1506, 2022.
- [20] S. Krishnan, M. Lam, *et al.*, "QuaRL: Quantization for fast and environmentally sustainable reinforcement learning," *IEEE Trans. Machine Learning Research*, 2022.
- [21] S. M. Cherati, M. Barzegar, and L. Sousa, "MSDF-Based MAC for Energy-Efficient Neural Networks," *IEEE Trans. VLSI Syst.*, pp. 1–12, Feb. 2025.
- [22] O. Kokane *et al.*, "LPRE: Logarithmic Posit-enabled Reconfigurable edge-AI Engine," *IEEE ISCAS*, 2025.
- [23] S. Azizi, M. Nazemi, M. Kamal, and M. Pedram, "Low-Precision Mixed-Computation Models for Inference on Edge," *IEEE Trans. Very Large Scale Integr. Syst.*, vol. 32, p. 1414–1422, Aug. 2024.
- [24] G. Raut, S. Karkun, and S. K. Vishvakarma, "An Empirical Approach to Enhance Performance for Scalable CORDIC-Based DNNs," *ACM Trans. Reconfigurable Technol. Syst.*, vol. 16, June 2023.
- [25] N. Ashar, G. Raut, V. Treevedi, *et al.*, "QuantMAC: Enhancing Hardware Performance in DNNs With Quantize Enabled Multiply-Accumulate Unit," *IEEE Access*, vol. 12, pp. 43600–43614, 2024.
- [26] R. Pilipović, P. Bulić, and U. Lotrič, "A two-stage operand trimming approximate logarithmic multiplier," *IEEE Trans. Circuits Syst. I*, vol. 68, no. 6, pp. 2535–2545, 2021.
- [27] X. Xie, J. Lin, Z. Wang, and J. Wei, "An Efficient and Flexible Accelerator Design for Sparse CNNs," *IEEE Trans. Circuits Syst. I*, vol. 68, no. 7, pp. 2936–2949, 2022.
- [28] D. T. Nguyen, H. Je, *et al.*, "ShortcutFusion: From Tensorflow to FPGA-Based Accelerator With a Reuse-Aware Memory Allocation for Shortcut Data," *IEEE Trans. Circuits Syst. I*, vol. 69, no. 6, pp. 2477–2489, 2022.
- [29] W. Lee, K. Kim, W. Ahn, *et al.*, "A Real-Time Object Detection Processor With XNOR-Based Variable-Precision Computing Unit," *IEEE Trans. VLSI Syst.*, vol. 31, no. 6, pp. 749–761, 2023.
- [30] B. Wu, T. Yu, K. Chen, and W. Liu, "Edge-Side Fine-Grained Sparse CNN Accelerator With Efficient Dynamic Pruning Scheme," *IEEE Trans. Circuits Syst. I*, vol. 71, no. 3, pp. 1285–1298, 2024.
- [31] W. Jiang, H. Yu, and Y. Ha, "A high-throughput full-dataflow mobilenetv2 accelerator on edge fpga," *IEEE Trans. Comput.-Aided Design Integr. Circuits Syst.*, vol. 42, no. 5, pp. 1532–1545, 2023.
- [32] S. Ki, J. Park, and H. Kim, "Dedicated FPGA Implementation of the Gaussian TinyYOLOv3 Accelerator," *IEEE Trans. Circuits Syst. II*, vol. 70, no. 10, pp. 3882–3886, 2023.
- [33] M. Kim, K. Oh, *et al.*, "A Low-Latency FPGA Accelerator for YOLOv3-Tiny With Flexible Layerwise Mapping and Dataflow," *IEEE Trans. Circuits Syst. I*, vol. 71, no. 3, pp. 1158–1171, 2024.
- [34] K. Li, M. Huang, A. Li, S. Yang, Q. Cheng, and H. Yu, "A 29.12-TOPS/W Vector Systolic Accelerator With NAS-Optimized DNNs in 28-nm CMOS," *IEEE Journal of Solid-State Circuits*, pp. 1–12, 2025.
- [35] F. Conti, D. Rossi, *et al.*, "A 12.4TOPS/W @ 136GOPS AI-IoT System-on-Chip with 16 RISC-V, 2-to-8b Precision-Scalable DNN Acceleration and 30%-Boost Adaptive Body Biasing," in *ISSCC*, pp. 21–23, 2023.
- [36] W. Lu, H.-H. Pei, *et al.*, "A 28nm Energy-Area-Efficient Row-based pipelined Training Accelerator with Mixed FXP4/FP16 for On-Device Transfer Learning," in *IEEE ISCAS*, pp. 1–5, 2024.
- [37] Y. Wang, D. Deng, *et al.*, "PL-NPU: An Energy-Efficient Edge-Device DNN Training Processor With Posit-Based Logarithm-Domain Computing," *IEEE Trans. Circuits Syst. I*, vol. 69, no. 10, pp. 4042–4055, 2022.